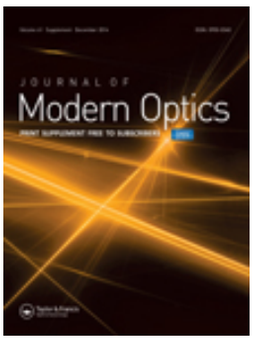

Journal of Modern Optics

ISSN: 0950-0340 (Print) 1362-3044 (Online) Journal homepage: http://www.tandfonline.com/loi/tmop20

New asymmetric propagation invariant beams obtained by amplitude and phase modulation in frequency space

J. Mendoza-Hernández, M.L. Arroyo Carrasco, M.M. Méndez Otero, S. Chávez-Cerda & M.D. Iturbe Castillo

To cite this article: J. Mendoza-Hernández, M.L. Arroyo Carrasco, M.M. Méndez Otero, S. Chávez-Cerda & M.D. Iturbe Castillo (2014) New asymmetric propagation invariant beams obtained by amplitude and phase modulation in frequency space, Journal of Modern Optics, 61:sup1, S46-S56, DOI: 10.1080/09500340.2014.935817

To link to this article: http://dx.doi.org/10.1080/09500340.2014.935817

Journal of Modern Optics, 2014
Vol. 61, No. S1, S46–S56, http://dx.doi.org/10.1080/09500340.2014.935817

New asymmetric propagation invariant beams obtained by amplitude and phase modulation in frequency space

J. Mendoza-Hernández[a]*, M.L. Arroyo Carrasco[a], M.M. Méndez Otero[a], S. Chávez-Cerda[b] and M.D. Iturbe Castillo[b]

[a]*Facultad de Ciencias Físico Matemáticas, Benemérita Universidad Autónoma de Puebla, Puebla, Mexico;* [b]*Instituto Nacional de Astrofísica, Óptica y Electrónica, Luis Enrique Erro # 1, Tonantzintla, Puebla, Mexico*

(*Received 19 January 2014; accepted 11 June 2014*)

In this paper, we demonstrate, numerically and experimentally that using the mask-lens setup used by Durnin to generate Bessel beams Durnin [Phys. Rev. Lett. 58, 1499 (1987)], it is possible to generate different kinds of propagation invariant beams. A modification in the amplitude or phase of the field that illuminates the annular slit is proposed that corresponds to modulation in frequency space. In particular, we characterize the new invariant beams that were obtained by modulating the amplitude of the annular mask and when the incident field was modulated with a one-dimensional quadratic or cubic phase. Experimental results using an amplitude mask are shown in order to corroborate the numerical predictions.

Keywords: propagation invariant beams; diffraction; modulating phase and amplitude

1. Introduction

Diffractionless or propagation invariant optical fields do not present spreading or change in their transverse intensity distribution as they propagate within a finite volume determined by the optical setup. One of the first reports of these propagating fields was done by Fujiwara [1] in 1962, while investigating the images of a reflecting axicon, where he clearly describes the propagation invariance as : *Since the distance does not appear in the argument of* J_0 [*the zero order Bessel function*], *it is obvious that the size of the diffraction image is always the same for any distance from the cone to its maximum range*. In a similar way, more than two decades later, the Spanish group lead by Gómez–Reino reported that refractive axicons can also produce transverse intensity distributions with propagation invariant properties [2]. When illuminated with a plane wave, either the reflective or the refractive axicon both produce conical waves.

It is interesting to note the very first report of a diffraction pattern with Bessel J_0 intensity distribution was done by G. B. Airy in 1840 in a study of the diffraction by an annular aperture. In his analysis, he does not refer to the Bessel function but uses numerical values of a, nowadays, known integral representation of it, possibly since Bessel function was not known as such at the time [3]. Follow-up studies have shown that annular apertures play a definite role for Bessel diffraction patterns and also can increase the depth of field of optical systems and, if illuminated with radially polarized light, can yield superresolution [4].

Twenty-five years later to Fujiwara, Durnin and co-workers used an Annular Slit and a Lens (ASL) separated by its focal distance to correct the diffracting wavefront transforming it into conical waves and hence producing a propagating invariant transverse Bessel intensity pattern that they called Bessel nondiffracting beam. From their theoretical analysis, they emphasized that the spectrum of a Bessel beam would lie on a ring what makes them to be related to conical waves [5–7].

Other propagation invariant beams had been reported since the generation of Bessel beams, high-order Bessel, Mathieu, and Parabolic beams [8–13]. These beams also have their spectrum on a ring and a characteristic modulating function that should be possible to create them using the ASL setup finding a way to modulate the annular aperture with the corresponding function.

There is another family of propagation invariant fields that propagate along parabolic trajectories, these are the Airy beams. Although not belonging to the same class of propagation invariant fields with conical waves described above, their main propagation features are similar and are easily understood using a traveling waves approach similar to that of Bessel beams since Airy functions belong to the family of Bessel functions [14]. Airy beams are bidimensional, with one longitudinal dimension and a transverse dimension. It is for this reason that, even though they are produced with a cubic phase, their intensity pattern is not the same as that produced by coma aberration in a two-dimensional transverse pattern.

*Corresponding author. Email: jobmendozah@alumnos.fcfm.buap.mx

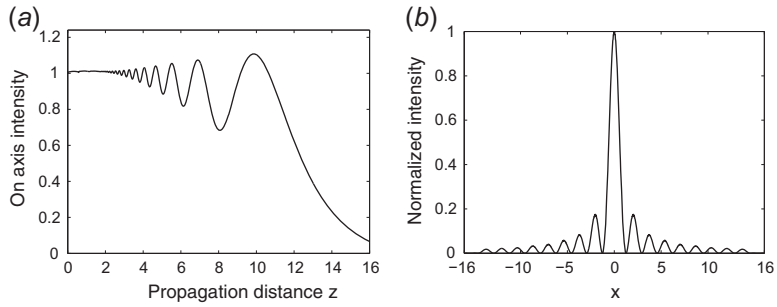

Figure 1. Numerical on-axis intensity (*a*) and intensity profile (*b*) for plane wave illumination of the ASL setup using an annular slit of radius 1, a lens of radius 16, and focal length of 1.

All of the propagation invariant fields mentioned above have the property of self-reconstruction. When they are partially obstructed, they recover its transverse distribution after some propagation distance [15,16]. It was believed that propagation invariant beams were the only field distributions with this property, but few years ago it was shown that diffractive caustic beams also present similar properties [17].

Recently, it was experimentally demonstrated [18] that phase modulation and amplitude modulation of the incident beam to an axicon produces very different intensity distribution, from that of the Bessel beam. In [19], the modulation in amplitude of the ASL setup with multiple apertures, regularly distributed in the aperture, produced propagation invariant distributions. However, until now it has not been analyzed in other field distributions created by modulating amplitude and particularly in phase, that can be obtained when the incident field is modulated at the aperture in an ASL setup, and must be propagation invariant.

In this work, we have made a numerical analysis of the beams generated when a modulation in the amplitude or in the phase of the incident field is introduced in the ASL setup. The modulation in amplitude is made to the annular mask with apertures not regularly distributed and the modulation in phase to the incident field is made considering a one-dimensional quadratic or cubic phase. It is shown that the obtained field distributions are diffractionless and their cross-section does not have rotational symmetry around the propagation axis. In some cases, caustic diffractionless distributions were obtained. We also present experimental generation of the field distributions obtained by some of the proposed modulations using an amplitude annular aperture illuminated with a He–Ne laser beam.

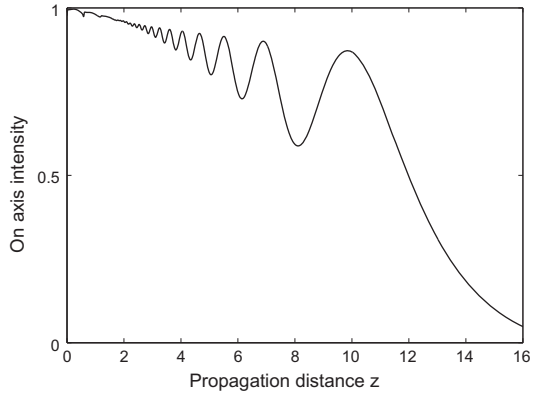

Figure 2. On-axis intensity, after the lens, for the beam generated with the ASL setup when incident field was modulated with a quadratic phase Δ_q. In this setup, an annular slit of radius 1 and focal length equal to 1 was used.

2. Analytical description of the ASL setup

The spatial evolution of the amplitude U of a propagation invariant beam along the z axis can be described by the following reduced Whitaker's integral [6]:

$$U(x,y,z) = \exp(ik_z z)\int_0^{2\pi} A(\phi)\exp\left(ik_t(x\cos(\phi) + y\sin(\phi))d\phi/2\pi, \quad (1)$$

where $A(\phi)$ is a complex function that lies on a ring of radius k_t, in frequency space. The transverse and longitudinal components of the wave vector satisfy the relation $k^2 = k_t^2 + k_z^2$, where $k = 2\pi/\lambda$ is the magnitude of the wave number and λ the wavelength of the field. Equation (1) is the fundamental solution that determines the propagation invariant fields if $A(\phi)$ is known. When $A(\phi)$ is a constant, the beam obtained is the zero-order Bessel beam, the function $A(\phi) = \exp(\mathrm{im}\phi)$ produces high-order Bessel beams with angular momentum or if $A(\phi) = \mathrm{ce}_m(\phi;q) + \mathrm{ise}_m(\phi;q)$ the resulting beams is mth-order Mathieu beams, where ce and se are the even and odd angular Mathieu functions and q is the ellipticity parameter [9,10]. Thus, it is this $A(\phi)$ defined on a ring in frequency space that determines the structure of the propagation invariant field and it will be the main subject of our investigation.

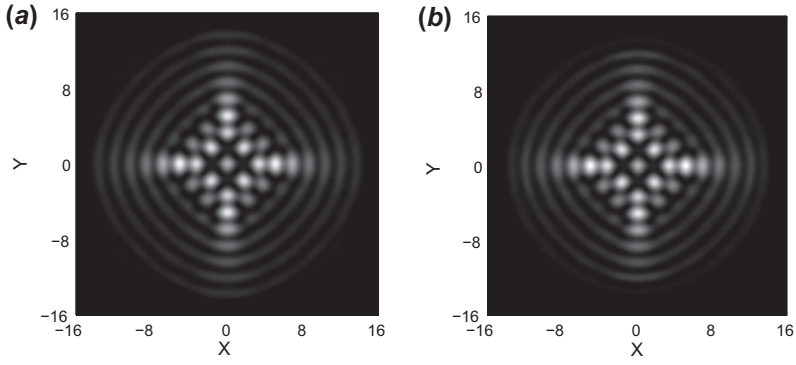

Figure 3. Numerical cross-section at $z = 1$ (*a*) and $z = 2$ (*b*) when incident field was modulated with a quadratic phase Δ_q.

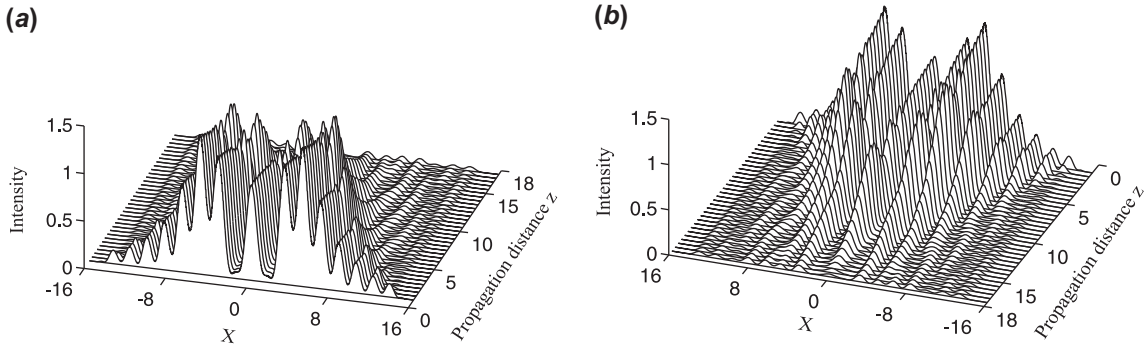

Figure 4. Central intensity profile evolution for the beam generated with the quadratic phase modulation Δ_q(*a*) and a rear view in (*b*).

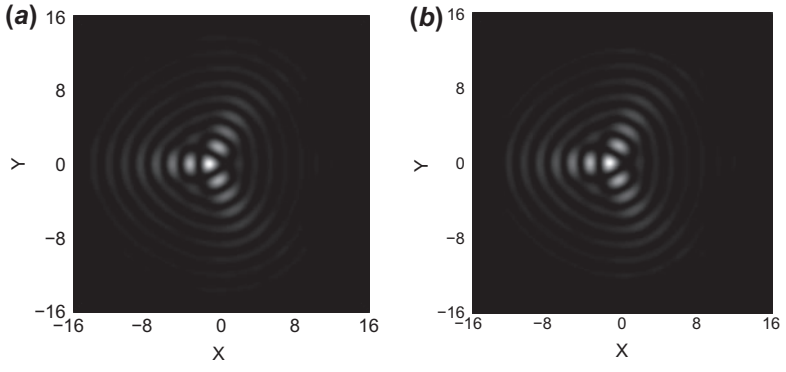

Figure 5. Numerical cross-section at propagation distances $z = 1$ (*a*) and $z = 2$ (*b*), when the incident field to the ASL setup was modulated with a cubic phase Δ_c.

Durnin and co-workers realized that Equation (1) could be implemented experimentally with an Annular Slit of infinitesimal width and a Lens (ASL), and illuminated with a plane wave setting $A(\phi) = \text{const}$ what makes the integral to be a representation of J_0 the zero-order Bessel function of the first type [5]. In detail, to generate a zero-order Bessel beam using the ASL setup we need a positive lens with focal length f and radius R set at the plane $z = 0$; a screen with an annular transmittance of radius b and infinitesimal width not larger than $0.1b$ that is placed at $z = -f$. When the screen is illuminated with a collimated light beam, the field after the lens is described by Equation (1). That field can be interpreted as a conical wave with vectors angled at

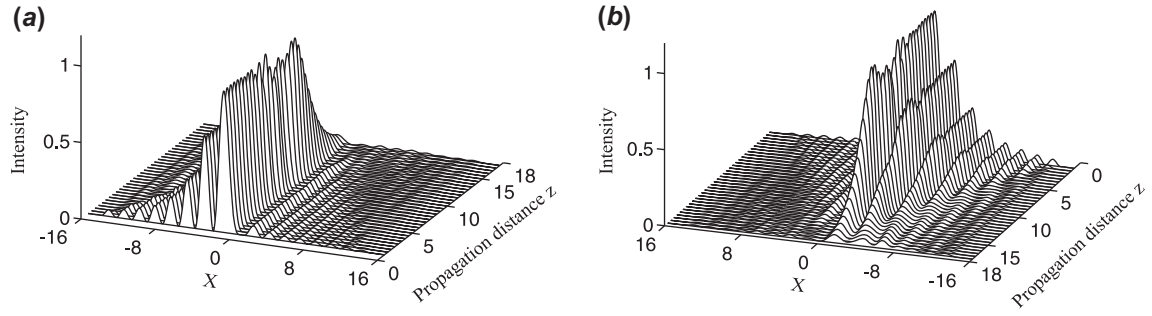

Figure 6. Central intensity profile evolution along x-coordinate when incident field was modulated with the cubic phase Δ_c (a) and a rear view in (b).

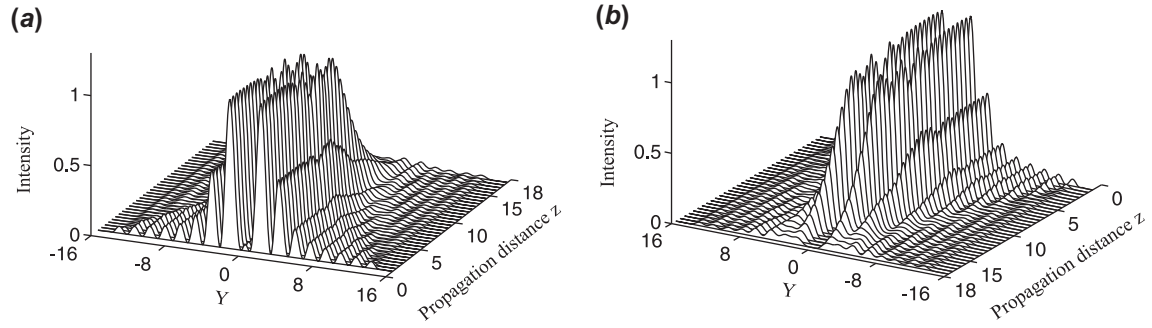

Figure 7. Central intensity profile evolution along y coordinate when incident field was modulated with the cubic phase $\Delta_c(a)$ and a rear view in (b).

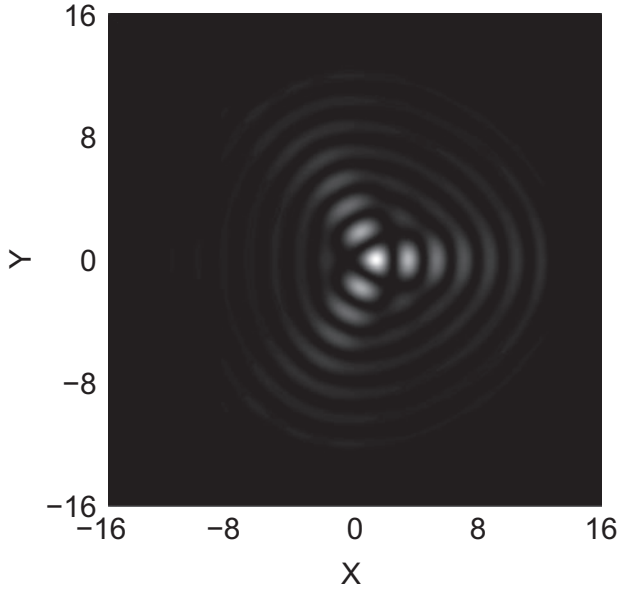

Figure 8. Cross-section at $z = 2$ when the incident field is modulated with the cubic phase as in Figure 5 but with the opposite sign.

$\theta = \tan^{-1}(k_t/k_z)$ to the z axis [7]. We notice that from the geometry of the ASL setup $k_t/k_z = b/f$ and within the paraxial approximation $k_t = 2\pi b/\lambda f$. Geometrically, the distance that the beam can be considered as propagation invariant is given by $Z_{\max} = R/\tan(\theta)$ [5].

In our case, instead of solving Equation (1) we approached the problem by the equivalent one of propagating an initial condition of amplitude- or phase-modulated field defined in a thin ring by means of the paraxial wave equation, then after some distance corresponding to the far field a positive lens with an adequate focal length is introduced. The field profiles after the lens were obtained at different propagating planes also monitoring the intensity behavior on axis. The equation was normalized in the transversal coordinate to a transverse parameter x_0 and in the propagation coordinate to L_D defined as $L_D = \pi x_0^2/\lambda$.

3. Numerical results

We initially simulate the ASL setup having as initial condition a plane wave that it is propagated through from an annular slit with radius $b = 1$ and width $\Delta b = 0.1$ and a thin spherical lens of focal length $F = 1$, and radius

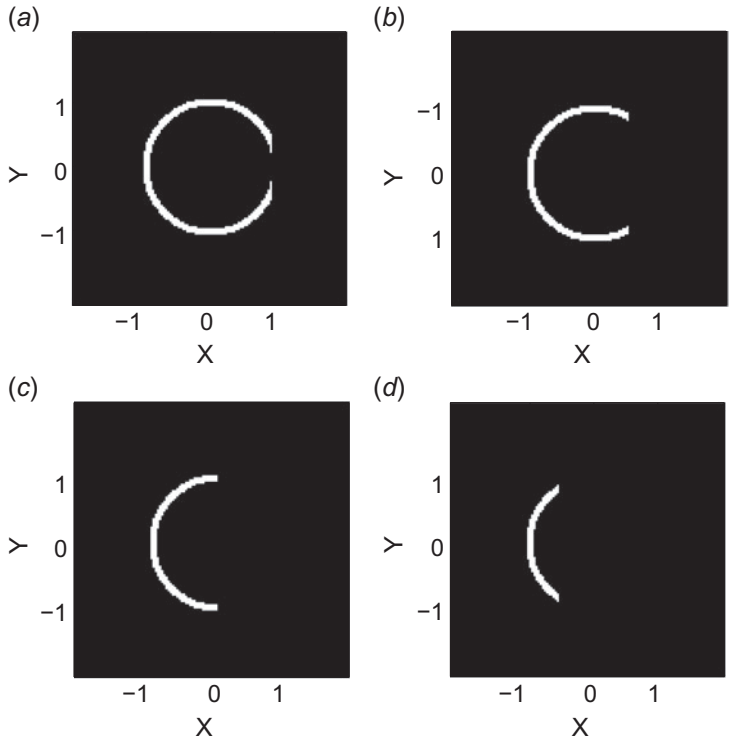

Figure 9. Mask used for amplitude modulation. The annular mask was partially covered with an opaque plane according to the next proportions of the radius: 0.1 (*a*), 0.5 (*b*), 1 (*c*), and 1.5 (*d*).

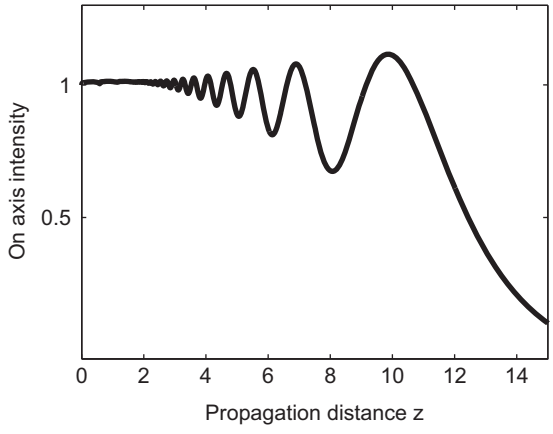

Figure 10. On-axis intensity later of lens, when the initial condition representing by Figure 9(*b*) was used in the ASL setup. For an annular mask of radius 1 and a lens of focal length of 1.

of $R = 16$. Under these conditions, the field generated after the lens was practically the zero-order Bessel beam, with on-axis intensity and the intensity profile as that shown in Figure 1.

As it is observed in Figure 1, the on-axis intensity initially is constant, then oscillates, and finally decays to a value of 0.1 at a distance of 16. The intensity profile has central lobe with a radius of 1.2, and eight concentric rings.

After this, we proceeded to study the effect of phase modulation in the incident field to the ASL setup. Two one-dimensional cases were considered: quadratic and cubic phase modulation. The one-dimensional quadratic phase was numerically modeled with the following function $\Delta_q(X, Y) = \exp(iX^2/F_p)$ and the one-dimensional cubic phase was modeled with $\Delta_c(X, Y) = \exp(iX^3/F_p)$, where F_p is the cylindrical focal length for the two-dimensional case and it becomes a cubic strength parameter for the cubic case and could be positive or negative.

The results obtained when the incident field to the mask was modulated with a quadratic phase Δ_q, with $F_p = 1/8$ are shown in Figures 2–4. The on-axis intensity of the generated beam is shown in Figure 2, where we can observe that it decreases, in a slow way, as the beam propagated but following a similar qualitative behavior to that obtained for the case without modulation (see Figure 1). The cross-section at two different positions is shown in Figure 3. As we can observe, the pattern does not presented the circular symmetry of the case without modulation, as expected from the phase function. It is interesting to note that changes in the sign of the phase modulation did not give remarkable differences in the pattern.

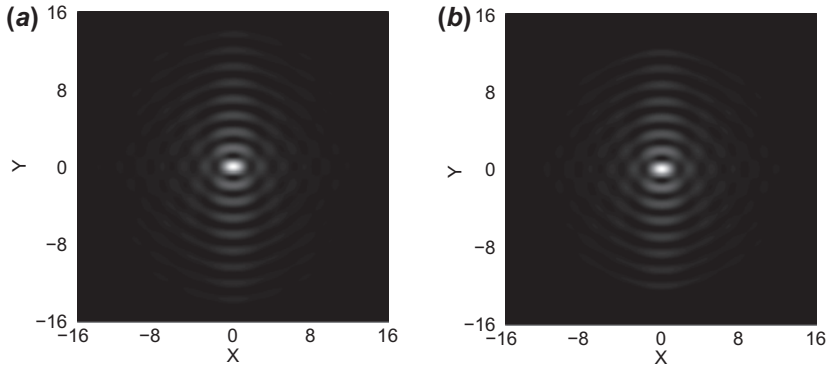

Figure 11. Numerical cross-section at propagation distances $z = 1$ (a) and $z = 2$ (b) when the initial condition representing by Figure 9(b) was used in the ASL setup.

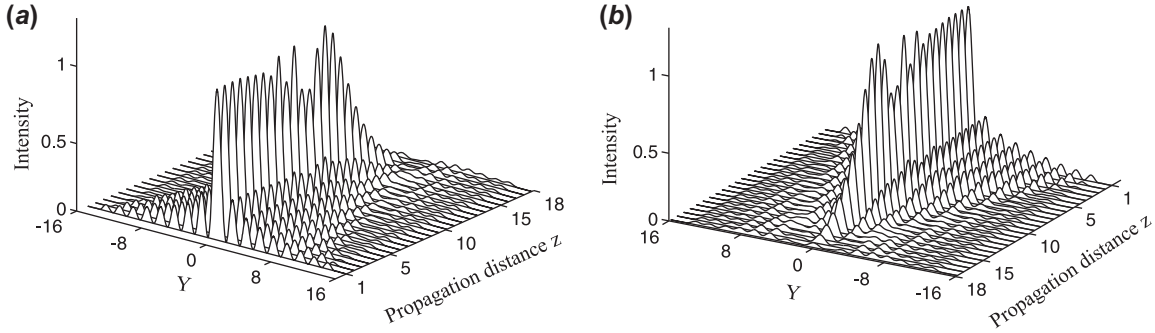

Figure 12. Central intensity profile evolution in the coordinate y when it was used the initial condition representing by Figure 9(b) (a) and a rear view in (b).

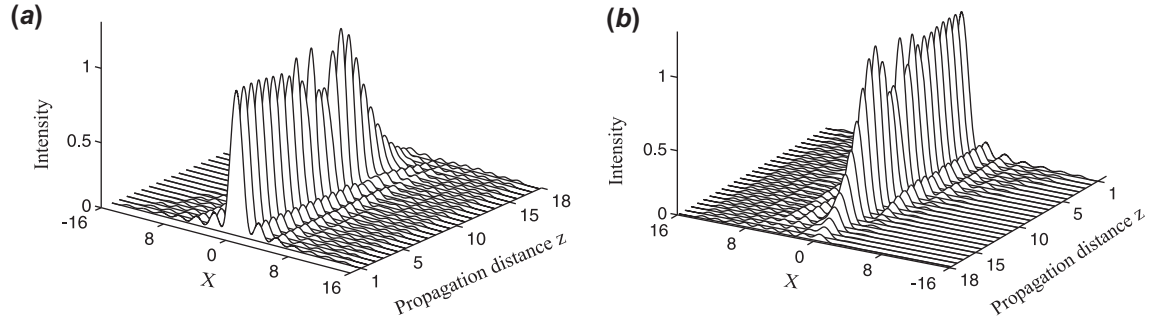

Figure 13. Central intensity profile evolution along x coordinate when it was used the initial condition representing by Figure 9(b) (a) and a rear view in (b).

The intensity profile evolution of this condition along the x–z plane is shown in Figure 4, where it is possible to observe the typical triangular-shape existence region of existence of a propagation invariant beam characteristic of conical wave fields [7].

Next, we present a very compelling behavior when the incident field was modulated with a one-dimensional cubic phase Δ_c with $F_p = 1/4$ as shown in Figures 5–8. The transverse patterns at two different positions are shown in Figure 5. The third-order power of the phase

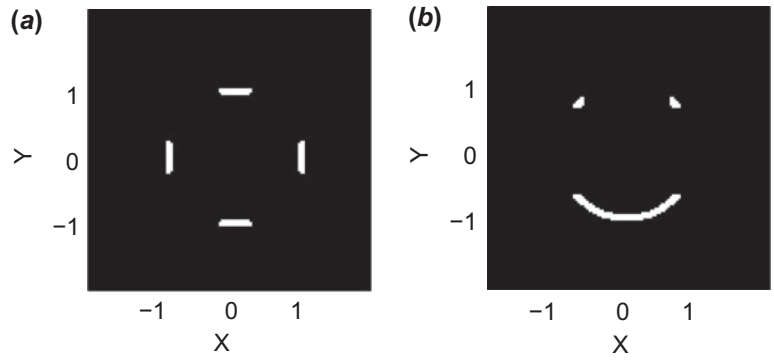

Figure 14. Initial conditions used for the modulation in amplitude of the mask-lens setup proposed by Durnin. The annular mask was covered sections of 0.7 (*a*) and 1.2 (*b*).

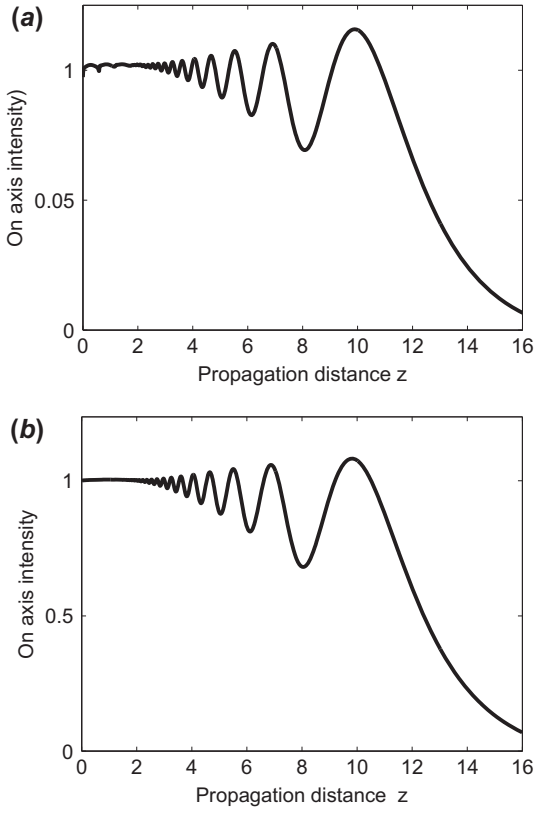

Figure 15. On-axis intensity after the lens when the masks represented in Figure 14(*a*) and Figure 14(*b*) is used in the ASL setup.

produces an intensity pattern that has a three-blade propeller shape. In Figures 6 and 7, we show the intensity profile evolution along the *x*–*z* and *y*–*z* planes, respectively. Once again, the typical evolution of a conical wave field can be observed. We observe that the center of the pattern is not on-axis but shifted along the *x* axis depending on the sign of the cubic strength parameter as can be observed in Figure 6.

When the sign of F_p is changed the cross-section rotates 180° with respect to the *z*-axis as it is shown in Figure 8. The propagation of such distribution followed the same behavior described for the opposite sign of F_p.

Now, we change to the modulation in amplitude of the incident field. This modulation was created by partially obstructing the annular mask. Examples of such modulation in amplitude are shown in Figure 9, where portions of 0.1, 0.5, 1, and 1.5 of the annular mask were covered.

As an example of the intensity distributions obtained with this type of initial condition, we present the results obtained with the mask of Figure 9(*b*). The behavior of the on-axis intensity, Figure 10, was very similar to that obtained for unobstructed annular mask, see Figure 1(*a*). In this case, the cross-section presented a central spot, noncircular, surrounded by bright zones that closely resembled the shape of a parabola, see Figure 11. The evolution of the intensity along the *x*–*z* plane and *y*–*z* plane are shown in Figures 12 and 13, respectively. The triangular zone typical of the conical beams was obtained.

Amplitude modulation equivalent having symmetric and asymmetric sections of the annular ring were also analyzed. This type of initial conditions is represented in the Figure 14. The behavior of the on-axis intensity, for both cases, was very similar to that obtained for unobstructed annular ring, see Figure 15. However, the cross-sections of both conditions did not presented rings; instead many bright spots were obtained, see Figure 16. When the mask represented by the Figure 14(*a*) was used, the cross-section presented a central array of nine bright spots, see Figure 16(*a*). This central intensity distribution is very similar to the obtained one, by the superposition of four plane waves making the same angle with the optical axis. For the initial condition represented by Figure 14(*b*), the cross-section consisted of bright spots distributed mainly along the *y* direction, see Figure 16(*b*).

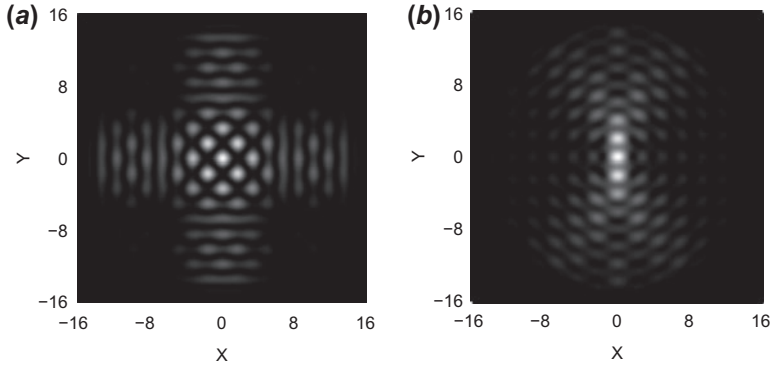

Figure 16. Cross-sections at $z = 1$, corresponding to the initial condition shown in: (*a*) Figure 14(*a*) and (*b*) Figure14(*b*).

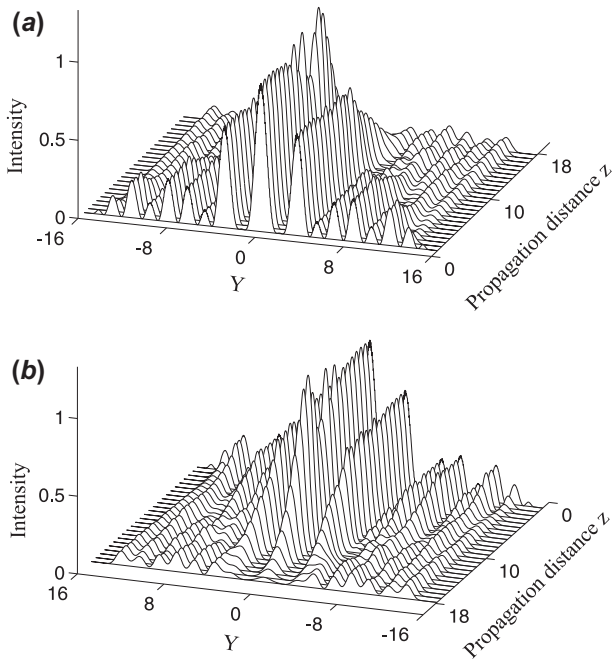

Figure 17. Central intensity profile evolution along the coordinate *y*, after the lens (*a*) for the initial condition represented in Figure 14(*a*) and a rear view in (*b*).

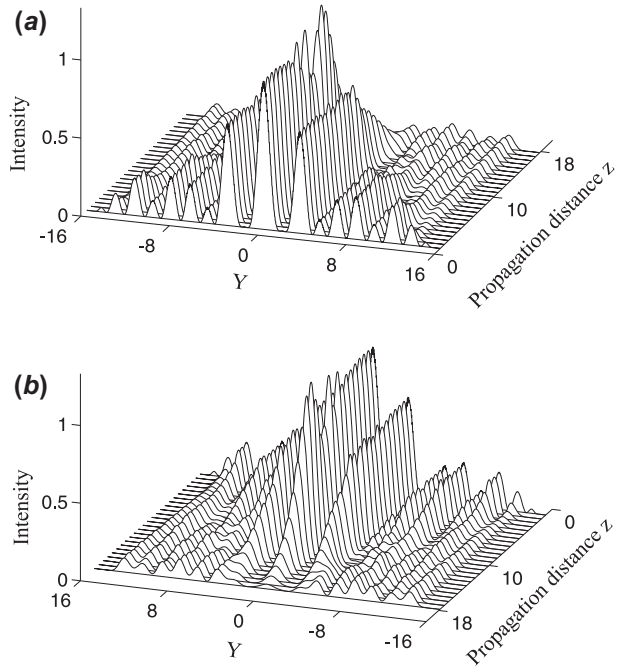

Figure 18. Central intensity profile evolution along the *y* coordinate when the initial condition represented in Figure 14(*b*) was used (*a*) and a rear view in (*b*).

The evolution of the central intensity profiles, of initial condition 14(*a*), after the lens is shown in Figures 17 where the typical behavior, of a propagation invariant beam is observed. For the initial condition represented in Figure 14(*b*), the behavior of the intensity was obtained along *y*, Figure 18, and *x*, Figure 19, axis. The intensity evolution along the *y* coordinate demonstrates that for this initial condition, the intensity is not symmetric, see Figure 19(*b*). However, the intensity evolution along the *x* coordinate is symmetric.

4. Experimental results

In this section, we present particular experimental results for some of the cases studied above that demonstrate the generation of propagation invariant beams obtained by phase or amplitude modulation of the incident field to the Annular-Slit-Lens setup. The beam from a 20 mW linear polarized He–Ne laser at 633 nm was spatially filtered and expanded. A quadratic phase modulation of the incident field was obtained using different focal length cylindrical lenses. Different masks were used to emulate the modulation in amplitude of the incident field. An annular mask of 0.1 mm of width and 1 mm of radii and a positive lens of 1 m of focal length and 12.7 mm of radii was used as the basic ASL setup. The Z_{max} with this condition is 12.7 m. The generated intensity distribution was captured with a CCD camera at different distances from the lens, see Figure 20.

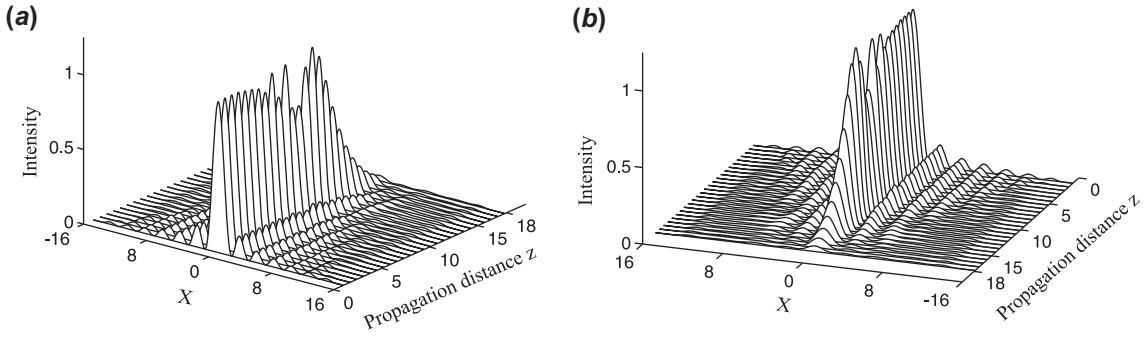

Figure 19. Central intensity profile evolution along x coordinate when the initial condition represented in Figure 14(b) was used (a) and a rear view in (b).

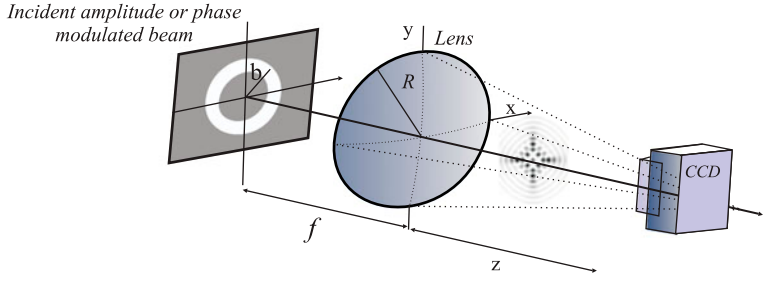

Figure 20. Schematic representation of the experimental setup for the generation of new propagation invariant beams modulating the incident field to the annular mask. (The colour version of this figure is included in the online version of the journal.)

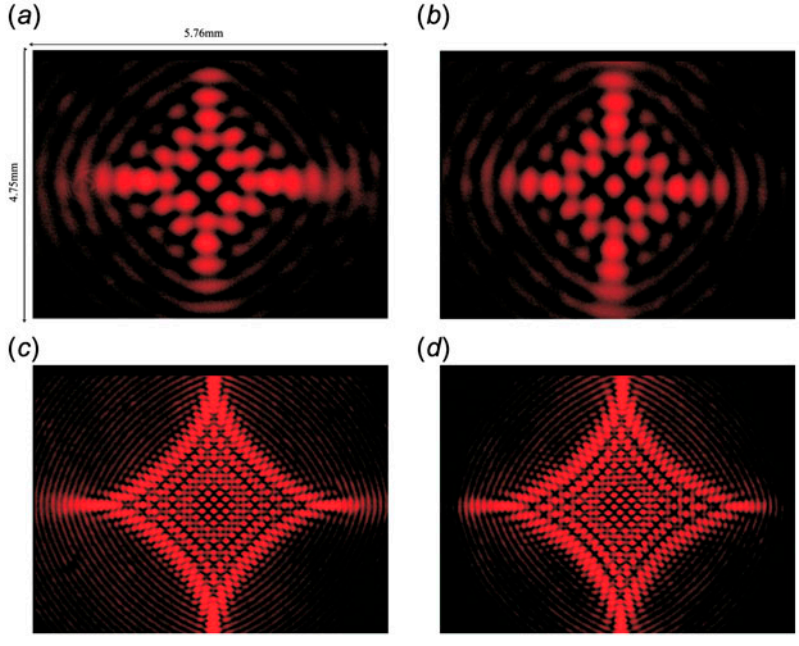

Figure 21. Experimental cross-sections obtained when the incident beam was modulated with a quadratic phase. When a 0.6 m cylindrical lens was used and propagation distances of: 0 m (a) and 3 m (b). When a 0.13 m cylindrical lens was used and propagation distances of: 0 cm (c) and 3 m (d). (The colour version of this figure is included in the online version of the journal.)

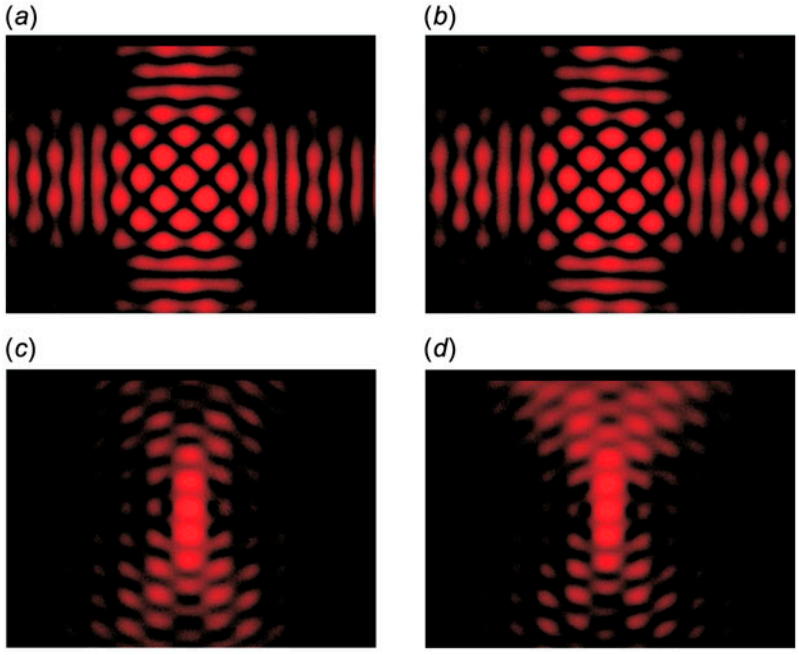

Figure 22. Experimental cross-sections obtained when the incident beam was modulated in amplitude. Distance after the lens of: 0 m ((*a*) and (*c*)) and 3 m ((*b*) and (*d*)). (The colour version of this figure is included in the online version of the journal.)

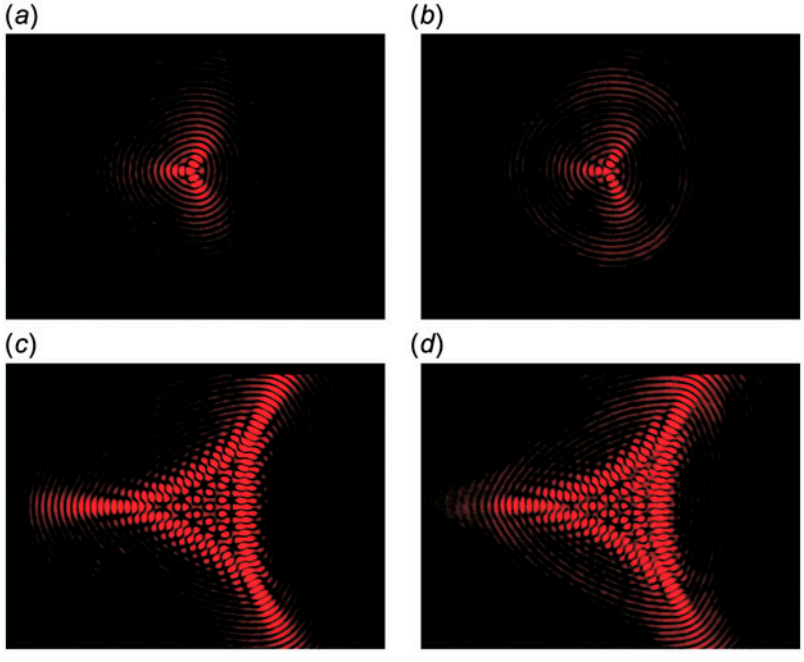

Figure 23. Experimental cross-sections obtained after the spherical lens when a cubic phase modulation was introduced to the incident beam. For a large (top) and a small (bottom) equivalent focal lens. Distance from the lens of: 0 cm (*a*) and (*c*) and 3 m (*b*) and (*d*). (The colour version of this figure is included in the online version of the journal.)

The intensity distributions generated after the lens with the quadratic phase modulation to the incident field are shown in Figure 21. Cylindrical lenses of 0.6 and 0.13 m of focal length were used. The wide-phase modulation produces a caustic beam with more structures than the narrow-phase modulation. The top and bottom images were obtained just after the lens and 3 m far from it. As it can be seen, the intensity distribution remained unchanged for several meters. After this distance, the central part of the distribution was the most resistant to changes. A comparison with Figure 3 demonstrates that the numerically predicted distribution was very similar to that obtained experimentally.

In the case of amplitude modulation of the incident field to the mask, we present the results obtained when as initial condition was used a mask as that represented in Figure 14. The images were obtained after the lens to a distance of 0 and 3 m. The top images correspond to a mask with four sectors regularly distributed. In this case, the cross-section presented a central array of nine bright spots. The bottom images correspond to the case when a mask, as that represented in Figure 14(*b*) was used. For this case, the experimental results demonstrate that the central part of the intensity distribution remained unchanged while the rest presented slight modifications, mainly due to the asymmetry of the initial condition. As can be seen, the numerically predicted distribution is very similar to that obtained experimentally (Figure 22).

Finally, we present experimental results when a cubic phase modulation was introduced in the beam that illuminated the annular mask. This phase modulation was obtained using a spatial light modulator. Two cases are presented. One for 1.26 m (top) and 0.17 m (bottom) of focal length of similar way that modulation of quadratic phase, see Figure 23. The images were taken at 0 and 3 m from the spherical lens. As we can observe, the intensity distribution of the top images is very similar to that calculated in the numerical section. The bottom images present a central region with a very complicated intensity distribution that remains practically invariant for several meters.

5. Conclusions

In this paper, we have demonstrated numerically and experimentally that with the Annular-Slit-Lens setup to generate propagation invariant fields, it is possible to generate new propagation invariant field distributions when modulation in phase or amplitude is added in frequency space. As a general characteristic of the intensity distribution, obtained with both types of modulation, is the lack of rings contrasted with Bessel beams for which some authors claim that they are the reason for the propagation invariance. In the case of a quadratic phase modulation, the intensity distribution is a caustic beam with the propagation invariant property. The results suggest the possibility to combine both types of modulations in order to generate propagation invariant beams with more complicated structures.

Acknowledgements

This paper is dedicated in memoriam of Vicente Iturbe Cordero (1928-2013). J. Mendoza-Hernández wants to thank CONACYT (México) for the fellowship that supported partially this work.

References

[1] Fujiwara, S. *J. Opt. Soc. Am.* **1962,** *52,* 287–292.
[2] Pérez, M.V.; Gómez-Reino, C.; Cuadrado, J.M. *Opt. Acta: Int. J. Opt.* **1986,** *33,* 1161–1176.
[3] Airy, G.B. *Philos. Mag. Ser.* **1841,** *3* (18), 1–10.
[4] Sheppard, C.J.R.; Choudhury, A. *Appl. Opt.* **2004,** *43,* 4322–4327; and references therein.
[5] Durnin, J.; Miceli, J.J.; Eberly, J.H. *Phys. Rev. Lett.* **1987,** *58,* 1499–1501.
[6] Durnin, J. *J. Opt. Soc. Am. A* **1987,** *4,* 651–654.
[7] Chávez-Cerda, S. *J. Mod. Opt.* **1999,** *46,* 923–930.
[8] Arlt, J.; Dholakia, K. *Opt. Commun.* **2000,** *177,* 297–301.
[9] Gutiérrez-Vega, J.C.; Iturbe-Castillo, M.D.; Chávez-Cerda, S. *Opt. Lett.* **2000,** *25,* 1493–1495.
[10] Gutiérrez-Vega, J.C.; Iturbe-Castillo, M.D.; Ramírez, G.A.; Tepichín, E.; Rodríguez- Dagnino, R.M.; Chávez-Cerda, S.; New, G.H.C. *Opt. Commun.* **2001,** *195,* 35–40.
[11] Hernández-Hernández, R.J.; Terborg, R.A.; Ricardez-Vargas, I.; Volke-Sepúlveda, K. *Appl. Opt.* **2010,** *49,* 6903–6909.
[12] Bandres, M.A.; Gutiérrez-Vega, J.C.; Chávez-Cerda, S. *Opt. Lett.* **2004,** *29,* 44–46.
[13] López Mariscal, C.; Bandres, M.A.; Gutiérrez-Vega, J.C.; Chávez-Cerda, S. *Opt. Express* **2005,** *13,* 2364–2369.
[14] Rogel-Salazar, J.; Jiménez-Romero, H.A.; Chávez-Cerda, S. *Phys. Rev. A* **2014,** *89,* 023807 and references therein.
[15] Bouchal, Z.; Wagner, J.; Chlup, M. *Opt. Commun.* **1998,** *151,* 207–211.
[16] Anguiano-Morales, M.; Mendez-Otero, M.M.; Iturbe-Castillo, M.D.; Chávez-Cerda, S. *Opt. Eng.* **2007,** *46* (078001), 1–9.
[17] Anguiano-Morales, M.; Martínez, A.; Iturbe-Castillo, M.D.; Chávez-Cerda, S.; Alcala-Ochoa, N. *Appl. Opt.* **2007,** *46,* 8284–8290.
[18] Anguiano-Morales, M.; Martínez, A.; Iturbe Castillo, M.D.; Chávez-Cerda, S. *Opt. Commun.* **2008,** *281,* 401–407.
[19] Chen, Y.F.; Liang, H.C.; Lin, Y.C.; Tzeng, Y.S.; Su, K.W.; Huang, K.F. *Phys. Rev. A* **2011,** *83* (053813), 1–4.